

Mixed Freeze-In and Freeze-Out Histories and Dark-Sector Decays in a \mathbb{Z}_4 Two-Scalar Model

J. P. Carvalho-Corrêa,^{*} B. A. Couto e Silva,[†] and B. L. Sánchez-Vega[‡]

Departamento de Física, UFMG, Belo Horizonte, MG 31270-901, Brazil.

(Dated: February 24, 2026)

We present a systematic non-equilibrium analysis of a renormalisable \mathbb{Z}_4 Higgs-portal dark sector comprising a complex scalar S_A and a real scalar S_B . In this framework, conversion, semi-annihilation, and (when kinematically allowed) $S_B \rightarrow S_A S_A$ decays shape the coupled relic-density evolution. Imposing theoretical consistency, Higgs invisible-decay limits, and the latest LZ spin-independent bound with the standard relic-fraction rescaling, we show that the severe exclusions typical of thermal two-WIMP analyses are largely an artefact of requiring *both* components to thermalise with the SM bath. Mixed WIMP–FIMP (and fully feeble FIMP–FIMP) histories reopen regions excluded in thermal two-WIMP interpretations, since the total relic density can be shared while the direct-detection signal is carried only by the thermal fraction. For the unstable hierarchy $M_{S_B} > 2M_{S_A}$, we identify decay-dominated regimes—SuperWIMP, injection-assisted freeze-out, and sequential freeze-in (“SuperFIMP”)—where late dark-sector injection sets the final S_A abundance. These results establish the \mathbb{Z}_4 Higgs-portal model as a controlled benchmark for multi-component dark matter beyond the two-thermal-relic assumption.

arXiv:2602.18564v1 [hep-ph] 20 Feb 2026

^{*} jpcarv-15897@ufmg.br

[†] brunoaces@ufmg.br

[‡] bruce@fisica.ufmg.br

CONTENTS

I. Introduction	3
II. The Model	4
III. Cosmological Evolution and Phenomenology	6
A. Boltzmann Equations	7
B. Direct Detection Constraints	10
C. Higgs Invisible Decay	10
D. Cosmological Constraints	11
1. Big Bang Nucleosynthesis	11
2. Lyman- α Forest	12
IV. Numerical Analysis and Results	12
A. Stable Scenarios	15
1. Pure Freeze-in: the FIMP–FIMP Regime	16
2. S_B (WIMP) diluted by S_A (FIMP)	18
3. S_A (WIMP) diluted by S_B (FIMP)	21
B. Unstable Scenarios	22
1. The SuperWIMP mechanism (WIMP parent)	23
2. Injection and sequential freeze-in with late dark-sector decays	24
V. Conclusions	27
Acknowledgments	28
A. Theoretical Constraints	29
1. Perturbative unitarity	29
2. Global bounded-from-below condition	30
3. Perturbativity	30
References	30

I. INTRODUCTION

A wide range of cosmological and astrophysical observations firmly establishes the existence of non-baryonic dark matter (DM), which dominates the matter budget of the Universe and plays a central role in structure formation, see Refs. [1–4]. Despite this robust gravitational evidence, the microscopic nature of DM remains unknown, see Refs. [5, 6]. Since the Standard Model (SM) offers no viable candidate, the DM puzzle remains one of the sharpest motivations for physics beyond the SM.

Theoretical benchmarks and experimental search strategies have traditionally focused on scenarios in which the dark sector is effectively described by a single stable particle, see e.g. Refs. [6–11]. Multi-component scenarios, however, are well motivated and arise naturally in frameworks where stability is enforced by symmetries larger than \mathbb{Z}_2 Refs. [12–18]. Beyond adding degrees of freedom, such constructions enable genuinely new number-changing dynamics, including semi-annihilation and dark-sector conversion, which can reshape the relic-density evolution and qualitatively alter phenomenological constraints Refs. [19–21]. This is particularly transparent in scalar extensions based on \mathbb{Z}_{2n} symmetries, where the charge assignments simultaneously determine stability and select the dominant production and depletion channels Refs. [22, 23].

In a recent dedicated study, Ref. [24] performed a systematic analysis of thermal two-component scalar DM in the \mathbb{Z}_4 , $\mathbb{Z}_6(13)$, and $\mathbb{Z}_6(23)$ realisations, combining updated direct-detection constraints with a consistent treatment of theoretical requirements such as boundedness from below, perturbative unitarity and perturbativity (including one-loop effects). Within this theoretically viable parameter space, the latest spin-independent limits from LZ Ref. [25], applied with the standard rescaling by the fractional abundance of each component, rule out large regions of the scan. Importantly, this is not merely a quantitative tightening of single-component bounds: in two-WIMP setups, parameter points can be excluded *collectively* even when each species would individually satisfy its own rescaled limit. The appearance of such configurations highlights a tension that is structural to the assumption that *both* components are thermal WIMPs, rather than to the \mathbb{Z}_{2n} framework itself. This raises a natural question: *Does LZ disfavour the model, or only the assumption that both components are thermal WIMPs?*

In this work we address this question within the \mathbb{Z}_4 two-scalar setup, which represents the lowest-order discrete realisation among the \mathbb{Z}_{2n} scenarios considered in Ref. [24], by relaxing thermal equilibrium for (at least) one species. Concretely, we study a *mixed* WIMP–FIMP regime in which one component undergoes standard freeze-out while the second is produced via freeze-in. To cover

the full range of non-equilibrium histories, we also include the fully non-thermal limit in which *both* scalars are produced via freeze-in (the FIMP–FIMP regime). We solve the coupled cosmological evolution and map the regions where the feebly coupled component, typically much less constrained by direct-detection searches, can alleviate the experimental tension while the WIMP component remains potentially testable. Our goal is twofold: (i) to determine which regions ruled out in the thermal two-WIMP picture become viable once non-equilibrium production is implemented consistently, and (ii) to chart how the viable parameter space is reshaped when moving from the two-WIMP assumption to mixed and fully freeze-in histories, identifying the mechanisms—conversion, semi-annihilation, and late dark-sector decays—that drive this reorganisation and open up new phenomenologically relevant territory.

While Ref. [24] surveyed several \mathbb{Z}_{2n} constructions, here we focus on the \mathbb{Z}_4 realisation as a controlled renormalisable benchmark that already captures the multi-component dynamics relevant to our question. This choice keeps the interpretation maximally transparent and allows us to isolate the impact of mixed thermal histories, including freeze-in and decay-mediated injection, without additional model-dependent structures that are not essential for our purpose.

The paper is organised as follows. In Sec. II we present the renormalisable \mathbb{Z}_4 scalar setup and identify the interactions relevant for annihilation into the SM, dark-sector conversion, semi-annihilation, and the decay $S_B \rightarrow S_A S_A$. In Sec. III we formulate the coupled Boltzmann system and summarise the phenomenological ingredients relevant for mixed thermal histories, including direct-detection and Higgs-invisible constraints, as well as the cosmological impact of late dark-sector decays. In Sec. IV we present our numerical analysis and discuss the resulting viable parameter space in both the stable and decay-mediated regimes. We summarise and conclude in Sec. V.

II. THE MODEL

We consider a renormalisable scalar extension of the SM invariant under a discrete \mathbb{Z}_4 symmetry, introduced in Ref. [23] as a minimal setup for two-component scalar dark matter. All SM fields are taken to be neutral under \mathbb{Z}_4 , while the particle content is augmented by a complex scalar S_A and a real scalar S_B . Denoting the \mathbb{Z}_4 generator by $\omega_4 = e^{i\pi/2}$, the new fields transform as

$$S_A \rightarrow \omega_4 S_A = i S_A, \quad S_B \rightarrow \omega_4^2 S_B = -S_B, \quad (1)$$

i.e. S_A carries charge 1 and S_B charge 2 (mod 4). These assignments ensure that the lightest \mathbb{Z}_4 -charged state(s) are stable, while allowing heavier dark states to decay into lighter \mathbb{Z}_4 -charged

particles when kinematically open. In particular, the symmetry admits the cubic interaction $S_A^2 S_B$ (and its Hermitian conjugate), which enables the decay/injection channel $S_B \rightarrow S_A S_A$ (and the CP-conjugate $S_B \rightarrow S_A^\dagger S_A^\dagger$) when $M_{S_B} > 2M_{S_A}$. This will play a central role in the non-equilibrium regimes discussed in Sec. III.

The most general renormalisable Lagrangian consistent with the SM gauge symmetry and these charge assignments is

$$\mathcal{L} = \mathcal{L}_{\text{SM}} + (\partial_\mu S_A^*)(\partial^\mu S_A) + \frac{1}{2}(\partial_\mu S_B)(\partial^\mu S_B) - V(H, S_A, S_B), \quad (2)$$

with scalar potential

$$\begin{aligned} V(H, S_A, S_B) = & -\mu_H^2 |H|^2 + \lambda_H |H|^4 - \mu_A^2 |S_A|^2 + \lambda_A |S_A|^4 - \frac{1}{2}\mu_B^2 S_B^2 + \lambda_B S_B^4 \\ & + \lambda_{HA} |H|^2 |S_A|^2 + \frac{1}{2}\lambda_{HB} |H|^2 S_B^2 + \lambda_{AB} |S_A|^2 S_B^2 \\ & + \frac{1}{2}(\mu_{S1} S_A^2 S_B + \lambda_{S4} S_A^4) + \text{h.c.} . \end{aligned} \quad (3)$$

Throughout this work we assume CP conservation in the scalar sector. In particular, we choose a basis where μ_{S1} and λ_{S4} are real, so that the last line of Eq. (3) is equivalently the real combination $\frac{\mu_{S1}}{2}(S_A^2 + (S_A^\dagger)^2)S_B + \frac{\lambda_{S4}}{2}(S_A^4 + (S_A^\dagger)^4)$.

For later use in the coupled Boltzmann system, it is convenient to highlight the interactions controlling the leading number-changing processes. The Higgs-portal couplings λ_{HA} and λ_{HB} connect S_A and S_B to the SM through Higgs exchange. The quartic coupling λ_{AB} mediates dark-sector conversion, $S_A S_A^\dagger \leftrightarrow S_B S_B$. Finally, the μ_{S1} term opens genuinely \mathbb{Z}_4 -specific channels, including semi-annihilation and decay/injection dynamics once the relevant thresholds are crossed. The relative importance of these mechanisms in the WIMP–FIMP and FIMP–FIMP regimes will be discussed in Sec. III.

After electroweak symmetry breaking (EWSB), the Higgs acquires a vacuum expectation value $\langle H \rangle = (0, v)^T / \sqrt{2}$. We focus on a \mathbb{Z}_4 -preserving vacuum with $\langle S_A \rangle = \langle S_B \rangle = 0$, which prevents mixing between the Higgs and the dark scalars. The physical masses are $M_h^2 = 2\lambda_H v^2$ and

$$M_{S_A}^2 = \frac{1}{2}\lambda_{HA} v^2 - \mu_A^2, \quad M_{S_B}^2 = \frac{1}{2}\lambda_{HB} v^2 - \mu_B^2. \quad (4)$$

In practice, we trade the quadratic terms for the physical masses. Our independent input parameters are the two dark masses (M_{S_A}, M_{S_B}) , the trilinear coupling μ_{S1} , and the six dimensionless couplings $(\lambda_A, \lambda_B, \lambda_{HA}, \lambda_{HB}, \lambda_{AB}, \lambda_{S4})$.

Theoretical consistency requires the scalar potential to be bounded from below (BFB) and the high-energy $2 \rightarrow 2$ scalar scattering amplitudes to satisfy perturbative unitarity. Following

Refs. [24, 26], a set of sufficient BFB conditions is

$$\lambda_H > 0, \quad \lambda_A - |\lambda_{S4}| > 0, \quad \lambda_B > 0, \quad (5)$$

together with the portal requirements

$$\bar{\lambda}_{AB} \equiv \lambda_{AB} + 2\sqrt{(\lambda_A - |\lambda_{S4}|)\lambda_B} > 0, \quad (6)$$

$$\bar{\lambda}_{HA} \equiv \lambda_{HA} + 2\sqrt{\lambda_H(\lambda_A - |\lambda_{S4}|)} > 0, \quad (7)$$

$$\bar{\lambda}_{HB} \equiv \lambda_{HB} + 2\sqrt{\lambda_H\lambda_B} > 0. \quad (8)$$

A global BFB condition involving all field directions is collected in Appendix A. We impose these BFB constraints at tree level, as our focus is the low-energy phenomenology relevant for the mixed WIMP–FIMP (and FIMP–FIMP) regimes.

Perturbative unitarity is enforced through the standard partial-wave bound on the eigenvalues of the $2 \rightarrow 2$ scalar scattering matrices, $|\mathcal{M}_i| \leq 8\pi$. The explicit constraints for the potential in Eq. (3), including the cubic equation whose roots yield the remaining eigenvalues, are summarised in Appendix A. All theoretical bounds are enforced point-by-point in our numerical analysis.

III. COSMOLOGICAL EVOLUTION AND PHENOMENOLOGY

The \mathbb{Z}_4 setup features a characteristic dark-sector phenomenology shaped by three interaction topologies, illustrated in Fig. 1: (i) **Higgs-portal couplings** [$\lambda_{Hi} \equiv (\lambda_{HA}, \lambda_{HB})$], which connect each dark scalar to the SM bath, governing annihilation into SM final states (when relevant) and setting the spin-independent direct-detection cross sections; (ii) **Dark-sector conversion** (λ_{AB}), mediating interconversion through $S_A S_A^\dagger \leftrightarrow S_B S_B$ and thereby redistributing the abundances between the two species; and (iii) **Semi-annihilation and decay/inverse-decay dynamics** (μ_{S1}), allowed by the \mathbb{Z}_4 charge assignments (and more generally by \mathbb{Z}_N symmetries with $N > 2$). In particular, μ_{S1} enables $2 \rightarrow 2$ semi-annihilation channels such as $S_A S_A \rightarrow S_B h$ (and CP-conjugate processes), and controls the two-body decay/inverse-decay processes $S_B \leftrightarrow S_A S_A$ (and $S_B \leftrightarrow S_A^\dagger S_A^\dagger$) whenever kinematically allowed. These channels enter the coupled Boltzmann system and determine how the relic abundance is partitioned among the dark states.

Whether the spectrum realises a one- or two-component dark matter scenario depends on the mass hierarchy. If $M_{S_B} < 2M_{S_A}$, the two-body decay $S_B \rightarrow S_A S_A$ is kinematically forbidden and both scalars can contribute to the present DM density. Conversely, if $M_{S_B} > 2M_{S_A}$, the decay $S_B \rightarrow S_A S_A$ becomes allowed (mediated by the μ_{S1} interaction), so that the late-time dark sector

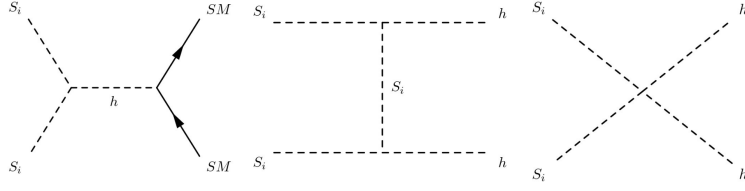
effectively reduces to a single surviving species S_A (with possible late injection from S_B decays). In this work, we investigate the general parameter space covering both hierarchies, including scenarios in which the two-field dark sector yields a single-component relic through late decays.

Regarding the production history, two limiting behaviours are relevant. If a component thermalises with the SM bath, its relic abundance is set by the usual freeze-out dynamics (WIMP-like). If it never thermalises, its population is gradually built up from the SM through freeze-in (FIMP-like). In what follows we are mainly interested in the *mixed* WIMP–FIMP regime, where intra-dark reactions can still redistribute the final abundances through conversion and semi-annihilation even when one component is produced non-thermally. The coupling ranges adopted in the numerical scan are specified in the numerical analysis below.

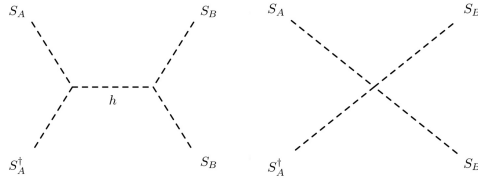
A. Boltzmann Equations

To determine the relic abundance of the dark sector, we track the cosmological evolution of the comoving number densities $Y_{S_i} = n_{S_i}/s$ as a function of $x = M_{S_A}/T$. We assume vanishing particle–antiparticle asymmetries in the dark sector, so that for the complex field S_A one has $Y_{S_A} = Y_{S_A^\dagger}$; for brevity we denote both by Y_{S_A} (and similarly for the equilibrium yields). In the collision terms, however, we keep the particle content explicit in the reaction labels: in particular, annihilation into the SM and conversion processes involving S_A are written with particle–antiparticle initial states, $S_A S_A^\dagger \leftrightarrow \dots$, while S_B is a real field. We write the collision terms in a form that vanishes in equilibrium, ensuring detailed balance channel by channel. Including all relevant number-changing processes, the coupled system reads:

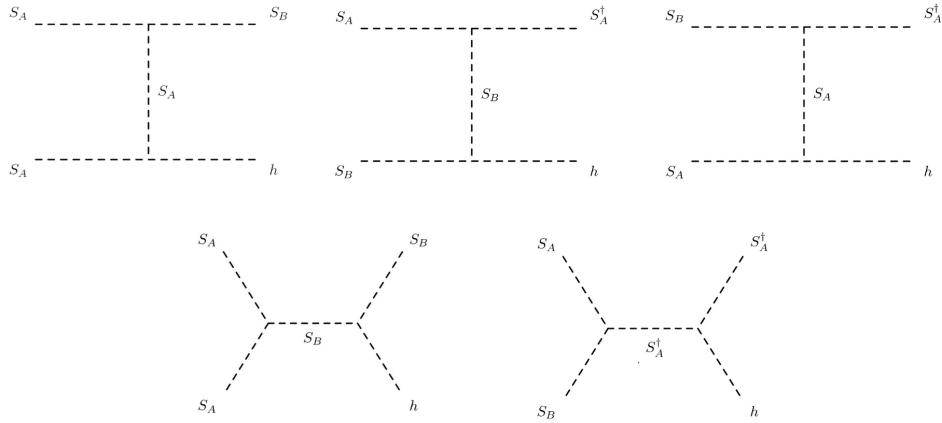
$$\begin{aligned} \frac{dY_{S_A}}{dx} = & -\sqrt{\frac{\pi}{45}} \frac{M_{\text{Pl}} g_*^{1/2} M_{S_A}}{x^2} \left[\langle \sigma v \rangle_{S_A S_A^\dagger \rightarrow \text{SM}} \left(Y_{S_A}^2 - Y_{S_A}^{\text{eq}2} \right) \right. \\ & + \langle \sigma v \rangle_{S_A S_A^\dagger \rightarrow S_B S_B} \left(Y_{S_A}^2 - Y_{S_B}^2 \frac{Y_{S_A}^{\text{eq}2}}{Y_{S_B}^{\text{eq}2}} \right) + 2 \langle \sigma v \rangle_{S_A S_A \rightarrow S_B h} \left(Y_{S_A}^2 - Y_{S_A}^{\text{eq}2} \frac{Y_{S_B}}{Y_{S_B}^{\text{eq}}} \right) \\ & \left. - \langle \Gamma_{S_B \rightarrow S_A S_A} \rangle \left(Y_{S_B} - Y_{S_A}^2 \frac{Y_{S_B}^{\text{eq}}}{Y_{S_A}^{\text{eq}2}} \right) \right], \end{aligned} \quad (9)$$



(a) Dark matter annihilation of the scalar states S_i ($i = A, B$) into SM final states via Higgs-portal interactions parameterized by λ_{Hi} .



(b) Conversion processes redistributing the abundances between components ($S_A S_A^\dagger \leftrightarrow S_B S_B$).



(c) Representative semi-annihilation channel enabled by the \mathbb{Z}_4 charge assignments ($S_A S_A \rightarrow S_B h$), together with its conjugate process $S_A^\dagger S_A^\dagger \rightarrow S_B h$.

FIG. 1: Key interaction topologies governing production, depletion, and redistribution of the two dark species in the coupled relic-density evolution.

$$\begin{aligned}
\frac{dY_{S_B}}{dx} = & -\sqrt{\frac{\pi}{45}} \frac{M_{\text{Pl}} g_*^{1/2} M_{S_A}}{x^2} \left[\langle \sigma v \rangle_{S_B S_B \rightarrow \text{SM}} \left(Y_{S_B}^2 - Y_{S_B}^{\text{eq}2} \right) \right. \\
& - 2 \langle \sigma v \rangle_{S_A S_A^\dagger \rightarrow S_B S_B} \left(Y_{S_A}^2 - Y_{S_B}^2 \frac{Y_{S_A}^{\text{eq}2}}{Y_{S_B}^{\text{eq}2}} \right) - 2 \langle \sigma v \rangle_{S_A S_A \rightarrow S_B h} \left(Y_{S_A}^2 - Y_{S_A}^{\text{eq}2} \frac{Y_{S_B}}{Y_{S_B}^{\text{eq}}} \right) \\
& \left. + \langle \Gamma_{S_B \rightarrow S_A S_A} \right) \left(Y_{S_B} - Y_{S_A}^2 \frac{Y_{S_B}^{\text{eq}}}{Y_{S_A}^{\text{eq}2}} \right) + \langle \sigma v \rangle_{S_B S_A \rightarrow S_A^\dagger h}^{\text{eff}} Y_{S_A} \left(Y_{S_B} - Y_{S_B}^{\text{eq}} \right) \right], \quad (10)
\end{aligned}$$

where M_{Pl} is the (non-reduced) Planck mass and $g_*^{1/2}$ denotes the standard combination of effective relativistic degrees of freedom entering $s/(Hx)$ (evaluated at the plasma temperature T). The thermally averaged decay rate is defined as the sum of the channels,

$$\langle \Gamma_{S_B \rightarrow S_A S_A} \rangle \equiv \left\langle \Gamma_{S_B \rightarrow S_A S_A} + \Gamma_{S_B \rightarrow S_A^\dagger S_A^\dagger} \right\rangle = \Gamma_{S_B}^{\text{tot}} \frac{K_1(x_{S_B})}{K_2(x_{S_B})}, \quad (11)$$

where K_n denotes the modified Bessel function of the second kind of order n . Here $x_{S_B} = M_{S_B}/T = (M_{S_B}/M_{S_A})x$ and $\Gamma_{S_B}^{\text{tot}} = 2\Gamma_{S_B \rightarrow S_A S_A}$ in the CP-symmetric limit. For notational economy, we express the conversion contribution in both equations using $\langle \sigma v \rangle_{S_A S_A^\dagger \rightarrow S_B S_B}$; the inverse reaction is automatically encoded by the equilibrium-subtracted structure enforcing detailed balance.

The scattering term written as $S_B S_A \rightarrow S_A^\dagger h$ is understood as a shorthand for the combined contribution of this channel and $S_B S_A^\dagger \rightarrow S_A h$, consistent with $Y_{S_A} = Y_{S_A^\dagger}$. Accordingly, we define

$$\langle \sigma v \rangle_{S_B S_A \rightarrow S_A^\dagger h}^{\text{eff}} \equiv \langle \sigma v \rangle_{S_B S_A \rightarrow S_A^\dagger h} + \langle \sigma v \rangle_{S_B S_A^\dagger \rightarrow S_A h}. \quad (12)$$

In this symmetric limit, this semi-annihilation topology only exchanges $S_A \leftrightarrow S_A^\dagger$ and thus does not affect the total S_A abundance, while it depletes/injects S_B , hence it appears explicitly only in Eq. (10).

For semi-annihilation we use $\langle \sigma v \rangle_{S_A S_A \rightarrow S_B h}$ for a single channel. The factor of 2 in Eq. (9) accounts for the two S_A quanta depleted per reaction, while the factor of 2 in Eq. (10) accounts for the sum of the channels $S_A S_A \rightarrow S_B h$ and $S_A^\dagger S_A^\dagger \rightarrow S_B h$ in the symmetric limit. In addition, whenever an annihilation channel involves two identical particles in the initial state (e.g. $S_B S_B$) we follow the standard symmetry-factor convention in the corresponding reaction densities.

Note that for a FIMP candidate (e.g., S_A with a tiny portal coupling $\lambda_{HA} \ll 1$), the abundance remains far below equilibrium, $Y_{S_A} \ll Y_{S_A}^{\text{eq}}$. In this limit, the portal-driven $S_A S_A^\dagger \leftrightarrow \text{SM}$ collision term effectively acts as a source proportional to $Y_{S_A}^{\text{eq}2}$, reproducing the usual freeze-in behaviour, while the coupled system captures the interpolation to the mixed regime once conversion and semi-annihilation become relevant.

B. Direct Detection Constraints

Direct-detection experiments probe the WIMP-like regions of parameter space through spin-independent (SI) scattering off nuclei induced by Higgs exchange. The SI DM–nucleon cross section can be approximated (at zero momentum transfer) by

$$\sigma_{S_i}^{\text{SI}} \approx \frac{f_N^2}{4\pi} \frac{\mu_{iN}^2 m_N^2}{M_h^4 M_{S_i}^2} \left(\frac{g_{hS_i S_i^{(\dagger)}}}{v} \right)^2, \quad (13)$$

where $\mu_{iN} = M_{S_i} m_N / (M_{S_i} + m_N)$ is the DM–nucleon reduced mass and we take $f_N \simeq 0.30$ for the effective scalar nucleon form factor. Here $g_{hS_i S_i^{(\dagger)}}$ denotes the trilinear Higgs–DM coupling in the broken phase. In our conventions, these couplings are

$$g_{hS_A S_A^\dagger} = \lambda_{HA} v, \quad g_{hS_B S_B} = \frac{\lambda_{HB}}{2} v. \quad (14)$$

In the multi-component scenario the predicted event rate scales with the local number density of each species. Assuming no spatial segregation, we approximate the local fractions by the cosmological relic-density fractions, $\xi_{S_i} \equiv \Omega_{S_i} h^2 / \Omega_{\text{DM}} h^2$. We implement the latest LZ bound Ref. [25] through the standard multi-component rescaling,

$$\sum_{i=A,B} \frac{\xi_{S_i} \sigma_{S_i}^{\text{SI}}}{\sigma_{\text{limit}}(M_{S_i})} < 1, \quad (15)$$

where $\sigma_{\text{limit}}(M_{S_i})$ denotes the single-component 90% C.L. upper limit at mass M_{S_i} . In our setup, $\sigma_{S_i}^{\text{SI}}$ is always negligible in the FIMP regime, so direct detection effectively constrains only the WIMP component.

For completeness, we comment on indirect-detection searches. We do not impose indirect-detection constraints in this work. In the FIMP regime, present-day annihilation signals are negligible due to the suppressed portal interactions. For the WIMP component, current limits are typically presented for annihilation into purely SM final states such as $b\bar{b}$, W^+W^- , or ZZ . In the \mathbb{Z}_4 scalar setup, however, the dominant (semi-)annihilation channels involve final states containing a Higgs boson and a dark scalar (e.g. $h + S_B$), so a reliable application of existing searches would require a dedicated recast. We therefore leave indirect-detection bounds for future work.

C. Higgs Invisible Decay

Additional constraints follow from Higgs-portal-induced invisible decays whenever one (or both) dark scalars satisfy $M_{S_i} < M_h/2$. In this case, the channels $h \rightarrow S_A^\dagger S_A$ and/or $h \rightarrow S_B S_B$ become kinematically accessible and contribute to the Higgs invisible branching ratio, $\beta_{\text{inv}} \equiv \text{BR}(h \rightarrow \text{inv})$.

Using the effective Higgs–DM coupling defined in Sec. III B, $\lambda_{Hi} \equiv g_{hS_iS_i^{(\dagger)}}/v$, the corresponding partial width can be written in the compact form

$$\Gamma_{h \rightarrow S_i S_i^{(\dagger)}} = \eta_{S_i} \frac{\lambda_{Hi}^2 v^2}{32\pi M_h} \left(1 - \frac{4M_{S_i}^2}{M_h^2}\right)^{1/2}, \quad (16)$$

with $\eta_{S_A} = 2$ for the complex scalar S_A (accounting for $S_A^\dagger S_A$) and $\eta_{S_B} = 1$ for the real scalar S_B (including the standard identical-particle symmetry factor in $S_B S_B$).

The total invisible branching ratio is obtained by summing all kinematically allowed invisible channels and is constrained to satisfy $\beta_{\text{inv}} \leq 0.107$ (0.077) at 95% C.L. (observed/expected), according to the ATLAS combination of Run 1 and Run 2 data Ref. [27].

This bound primarily constrains regions of parameter space with sizeable Higgs portal couplings and light dark scalars with $M_{S_i} < M_h/2$. In the FIMP regime, the portal interaction is feeble, and the constraint is therefore easily satisfied.

D. Cosmological Constraints

It is also important to comment on the cosmological impact of the late decay $S_B \rightarrow S_A S_A$. Since this process occurs entirely within the dark sector, the standard bounds on unstable relics associated with electromagnetic or hadronic energy injection during or after Big Bang Nucleosynthesis (BBN) are not directly applicable. Nevertheless, long-lived dark states may still be constrained indirectly if they (i) contribute a non-negligible energy density around $T \sim \mathcal{O}(\text{MeV})$, modifying the expansion rate during BBN, or (ii) produce a non-thermal population of S_A with sizable free streaming, potentially affecting structure formation and being constrained by Lyman- α forest data. In what follows we briefly justify why, in our setup and for the viable parameter space, both effects are negligible.

1. Big Bang Nucleosynthesis

BBN constraints on long-lived particles typically arise when late decays inject energetic photons and/or hadrons into the primordial plasma, thereby modifying light-element abundances (see e.g. Refs. [28–30] for reviews and classic analyses). In the present \mathbb{Z}_4 model, however, the decay $S_B \rightarrow S_A S_A$ (and its CP-conjugate) contains no SM particles in the final state, so the usual electromagnetic/hadronic injection limits do not apply.

A residual effect could only arise indirectly. First, the decay-produced S_A population could transfer energy to the visible bath via the Higgs portal; in the regions where S_A behaves as a FIMP (and where S_B is correspondingly long-lived), the portal coupling is feeble and the interaction rates are too small to efficiently thermalize or heat the plasma at $T \sim \mathcal{O}(\text{MeV})$. Second, a metastable S_B population could in principle affect BBN through its contribution to the total energy density (and hence to H). In our viable points, however, the energy density stored in S_B remains subdominant at the onset of nucleosynthesis, so the expansion history is not appreciably modified. We thus conclude that BBN does not impose additional constraints in our setup.

2. Lyman- α Forest

Dark matter produced in late decays can carry a non-thermal momentum distribution and behave as a “warm” subcomponent, potentially suppressing the matter power spectrum on small scales. Lyman- α forest data are sensitive to such effects, and the resulting constraints can be phrased in terms of the fractional abundance of the decay-produced component (see e.g. Refs. [31–33] and references therein). In our case, the relevant quantity is the fraction of dark matter originating from $S_B \rightarrow S_A S_A$ decays,

$$f_{\text{dec}} \equiv \frac{\Omega_{S_A}^{\text{dec}}}{\Omega_{\text{DM}}}, \quad (17)$$

where $\Omega_{S_A}^{\text{dec}}$ denotes the relic abundance of the decay-produced S_A population.

In our numerical scan we find $f_{\text{dec}} \ll 1$ for all viable points, so any decay-produced non-thermal component is too small to generate an observable suppression of small-scale structure, independently of the decay time or the mass splitting. The dominant contribution to the relic abundance instead arises from early-time production and behaves as standard cold dark matter. We therefore conclude that Lyman- α constraints are naturally satisfied and do not further restrict the viable parameter space.

IV. NUMERICAL ANALYSIS AND RESULTS

In this section we delineate the viable parameter space of the \mathbb{Z}_4 model and quantify the interplay between thermal freeze-out and non-thermal freeze-in production. To keep the scan focused on the relevant dark-sector dynamics, we fix a subset of input parameters to benchmark values. Standard-Model quantities are set to their PDG values (see Ref. [5]). Likewise, the quartic couplings that mainly control the vacuum structure and theoretical consistency (λ_A , λ_B , and λ_{S_4}) are fixed to

representative values that satisfy bounded-from-below conditions, perturbativity, and unitarity. In the regimes of interest, these self-couplings play a subleading role in the relic-density determination compared to the portal, conversion, and semi-annihilation interactions.¹

The numerical scan focuses on the parameters governing the dark-sector dynamics. The adopted ranges are summarised in Table I. We scan the mass of the complex scalar S_A in the range $40 \text{ GeV} \leq M_{S_A} \leq 2 \text{ TeV}$, covering the mass window relevant for current direct-detection searches. The range for the real scalar S_B is set according to the mass hierarchy: it is capped at $2M_{S_A}$ in stable two-component scenarios (to ensure the kinematic stability of S_B), and extended up to 4 TeV when the decay channel $S_B \rightarrow S_A S_A$ is open.

Following the WIMP-like/FIMP-like terminology introduced in Sec. III, we partition the Higgs-portal couplings according to the assumed thermal history of each component S_i ($i = A, B$). Concretely, we scan the portal parameters λ_{HA} and λ_{HB} in different ranges depending on whether the corresponding component thermalises (WIMP-like) or remains out of equilibrium (FIMP-like):

- **WIMP-like regime:** for a component that thermalises with the SM bath, we scan $\lambda_{Hi} \in [10^{-4}, 1]$, where λ_{Hi} stands for λ_{HA} (for S_A) or λ_{HB} (for S_B).
- **FIMP-like regime:** for a component produced via freeze-in, we restrict $\lambda_{Hi} \in [10^{-12}, 10^{-8}]$, as in Refs. [15, 34], with the same identification $\lambda_{Hi} = \lambda_{HA}$ or λ_{HB} .

When translating these parameters to Higgs-mediated observables (direct detection and invisible Higgs decays), we use the broken-phase couplings $g_{hS_i S_i}$ defined in Sec. III B.

A crucial consistency requirement is to preserve the non-thermal nature of the FIMP component. If intra-dark couplings are too large, reactions involving the WIMP component can populate the feeble sector efficiently enough to drive it towards thermal equilibrium, leading to a qualitatively different regime (often dubbed “dark freeze-out”). To avoid this, we restrict intra-dark interactions to small values while still allowing conversion and semi-annihilation to impact the final abundance partition. Concretely, we scan the conversion coupling in the range $\lambda_{AB} \in [10^{-12}, 10^{-8}]$ and take the trilinear parameter in $\mu_{S1} \in [10^{-8}, 10^{-1}] \text{ GeV}$.

We perform the numerical calculations with `micrOMEGAs` 6.0 (see Ref. [35]), using its multi-component routines to solve the coupled Boltzmann system. The model is considered viable if the total relic abundance, $\Omega_{\text{tot}} h^2 = \Omega_{S_A} h^2 + \Omega_{S_B} h^2$, agrees with the Planck 2018 value within a 2σ experimental interval enlarged by a conservative 10% theory uncertainty added in quadrature,

¹ For reproducibility, the benchmark choice for $(\lambda_A, \lambda_B, \lambda_{S_A})$ is stated in Table I.

TABLE I: Parameter ranges adopted in the numerical scan. The coupling range for the Higgs-portal parameters λ_{HA} and λ_{HB} depends on the assumed thermal nature (WIMP vs FIMP) of the corresponding component S_i . Intra-dark couplings (λ_{AB}, μ_{S1}) are kept small to preserve the non-thermal nature of the FIMP component.

Parameter	Scanning Range	Physical Role
<i>Mass parameters</i>		
M_{S_A}	[40, 2000] GeV	DM mass
M_{S_B}	[40, $M_{S_B}^{\max}$] GeV	DM or parent mass
<i>Conditions: $M_{S_B}^{\max} = 2M_{S_A}$ (stable) or 4000 GeV (unstable)</i>		
<i>Higgs portal couplings</i>		
λ_{HA} or λ_{HB} (WIMP-like S_i)	$[10^{-4}, 1]$	Thermal contact (freeze-out)
λ_{HA} or λ_{HB} (FIMP-like S_i)	$[10^{-12}, 10^{-8}]$	Feeble contact (freeze-in)
<i>Dark sector couplings</i>		
λ_{AB}	$[10^{-12}, 10^{-8}]$	Dark-sector conversion
μ_{S1}	$[10^{-8}, 10^{-1}]$ GeV	Semi-annihilation / decay
<i>Fixed parameters</i>		
$\lambda_A, \lambda_B, \lambda_{S4}$	(0.03, 0.02, 0.01)	Vacuum structure

imposed as

$$|\Omega_{\text{tot}} h^2 - \Omega_{\text{Planck}} h^2| \leq 2\sqrt{(\sigma_{\text{Planck}})^2 + (0.1 \Omega_{\text{Planck}} h^2)^2}. \quad (18)$$

We apply all vacuum-stability and perturbative-unitarity bounds discussed in Sec. II and detailed in Appendix A, and impose the latest spin-independent direct-detection constraints from LZ Ref. [25].

The \mathbb{Z}_4 symmetry admits a variety of cosmological histories depending on the mass hierarchy and on whether each scalar is in thermal contact with the SM bath. To organise the parameter space, we classify our scan into six benchmark scenarios, summarised in Table II. They cover all permutations of WIMP/FIMP assignments and the two qualitatively distinct regimes: a stable two-component spectrum ($M_{S_B} < 2M_{S_A}$) and a decay-mediated one-component spectrum ($M_{S_B} > 2M_{S_A}$).

Our analysis proceeds in two steps:

1. **Stable regime (Scenarios 1–3):** For $M_{S_B} < 2M_{S_A}$ both scalars are stable and can contribute to the present-day density. Scenario 1 provides a reference case where both components are produced via freeze-in (FIMP+FIMP). Scenarios 2 and 3 realise mixed histories (FIMP+WIMP and WIMP+FIMP, respectively), allowing us to test whether direct-detection bounds can be evaded when the WIMP component constitutes only a fraction of the total relic abundance (through the standard ξ -rescaling of the event rate).

2. **Decay-mediated regime (Scenarios 4–6):** For $M_{S_B} > 2M_{S_A}$ the decay $S_B \rightarrow S_A S_A$ becomes kinematically allowed (through the same \mathbb{Z}_4 -allowed interaction responsible for semi-annihilation), so that only S_A survives as the asymptotic relic. Scenario 4 corresponds to the classic superWIMP mechanism, in which a WIMP-like parent freezes out and subsequently decays into a feebly coupled daughter. Scenarios 5 and 6 capture complementary decay-driven histories in which S_A receives an additional non-thermal contribution from $S_B \rightarrow S_A S_A$: Scenario 5 realises an injection into a WIMP-like daughter, while Scenario 6 corresponds to purely feeble sequential production. Although subdominant in part of the parameter space, these late injections can be phenomenologically relevant by reshaping the final abundance partition and the momentum distribution of the surviving relic.

A. Stable Scenarios

We begin with the stable configurations, corresponding to the mass hierarchy $M_{S_B} < 2M_{S_A}$. In this regime the two-body decay $S_B \rightarrow S_A S_A$ is kinematically forbidden, so both species are cosmologically stable and may contribute to the present dark matter abundance.

Guided by Table II, we consider Scenarios 1–3. We start from the purely feeble case in which both components are produced via freeze-in (FIMP–FIMP), and then move to mixed realisations where one component behaves as a WIMP and the other as a FIMP, treating separately the cases in which the WIMP role is played by S_B (Scenario 2) or by S_A (Scenario 3).

A key aspect of the mixed regimes is the interplay between freeze-out, freeze-in, and intra-dark processes, which can reshuffle the relic-density partition through conversion and semi-annihilation. This can weaken direct-detection constraints compared to the single-component WIMP limit via the usual ξ -rescaling of the event rate.

TABLE II: Classification of the dark-sector scenarios investigated in this work. The ‘‘Nature’’ column indicates the coupling regime (WIMP/FIMP) of S_A and S_B , ‘‘Stability’’ specifies whether S_B can decay into $S_A S_A$, and ‘‘Mechanism’’ summarises the dominant production history.

Scenario	Nature (S_A, S_B)	Stability	Mechanism	Physical feature
<i>Stable regime: S_B stable</i> ($M_{S_B} < 2M_{S_A}$)				
1	FIMP + FIMP	Stable	Pure freeze-in	Two stable FIMPs; relic density is the dominant constraint.
2	FIMP + WIMP	Stable	Mixed	Two-component DM with a potentially subdominant WIMP fraction; direct-detection bounds apply with ξ rescaling.
3	WIMP + FIMP	Stable	Mixed	As in Scenario 2 but with the WIMP role assigned to S_A (and the FIMP to S_B).
<i>Decay-mediated regime: S_B unstable</i> ($M_{S_B} > 2M_{S_A}$)				
4	FIMP + WIMP	$S_B \rightarrow S_A S_A$	SuperWIMP	WIMP-like parent freezes out and later decays into a feebly coupled daughter.
5	WIMP + FIMP	$S_B \rightarrow S_A S_A$	Injection	FIMP-like parent injects S_A ; phenomenology close to a WIMP with an additional non-thermal contribution.
6	FIMP + FIMP	$S_B \rightarrow S_A S_A$	Sequential freeze-in	S_A receives a subleading contribution from the freeze-in and subsequent decay of S_B .

1. Pure Freeze-in: the FIMP–FIMP Regime

We start from the scenario in which both dark scalars behave as feebly interacting massive particles (FIMPs), as in Ref. [36]. In this regime the Higgs-portal couplings satisfy $\lambda_{HA}, \lambda_{HB} \lesssim 10^{-8}$ (within our scan ranges), preventing thermalisation with the SM bath. The relic abundances of S_A and S_B are then generated through freeze-in.

Since both components are stable, the present dark matter density is shared between the two species. For the viable points in this regime, direct and indirect searches do not provide relevant constraints because the portal couplings are extremely suppressed. The phenomenology is therefore governed mainly by the cosmological requirement on the total relic abundance and by how it is partitioned between S_A and S_B .

The viable parameter space is shown in Fig. 2. The left panel illustrates that the single-component freeze-in behaviour for S_A is recovered when it dominates the total abundance, $\Omega_{S_A}/\Omega_{\text{tot}} \rightarrow 1$, where $\Omega_{\text{tot}} \equiv \Omega_{S_A} + \Omega_{S_B}$, in agreement with the trends found in single-FIMP studies (see, e.g., Fig. 6 of Ref. [37]). A qualitatively different regime appears when both particles contribute comparably, $\Omega_{S_A} \simeq \Omega_{S_B}$.

As shown in the right panel of Fig. 2, this balanced configuration induces a pronounced correlation between the two portal couplings. Since freeze-in yields parametrically $\Omega_{S_i} h^2 \propto \lambda_{Hi}^2$ (up to a mild mass and phase-space dependence), comparable relic abundances typically require portal couplings of the same order, $\lambda_{HA} \sim \lambda_{HB}$ within $\mathcal{O}(1)$ factors, producing the curved band observed in the $(\lambda_{HA}, \lambda_{HB})$ plane. A similar feature was identified in Ref. [36] for two-component freeze-in scenarios.

It is instructive to contrast this behaviour with the multi-component *two-WIMP* realisations analysed in \mathbb{Z}_{2n} -stabilised scenarios, which provided part of the motivation for the present study. In the parameter scans of Refs. [23, 24], where both components thermalise with the SM bath and undergo freeze-out, the total relic density is often effectively dominated by a single species, with the second component remaining subdominant (see, e.g., Fig. 4 of Ref. [24] and Figs. 4 and 5 of Ref. [23]). By contrast, in the present \mathbb{Z}_4 FIMP–FIMP realisation both particles can naturally account for comparable fractions of the observed dark matter abundance.

As a consequence, regions that would fail to reproduce Ω_{DM} in a single-component freeze-in interpretation can become viable once the second FIMP component is included. In fact, even in a fully non-thermal FIMP–FIMP setup both states can contribute an appreciable share of the present dark-matter density, in sharp contrast to the two-WIMP case, where accommodating the observed abundance with *both* components typically clashes with direct-detection bounds. We thus find that a fully feebly interacting, multi-component dark sector can match the observed relic abundance while remaining effectively unconstrained by current terrestrial searches, with correlated portal couplings emerging as a characteristic feature of the balanced freeze-in regime.

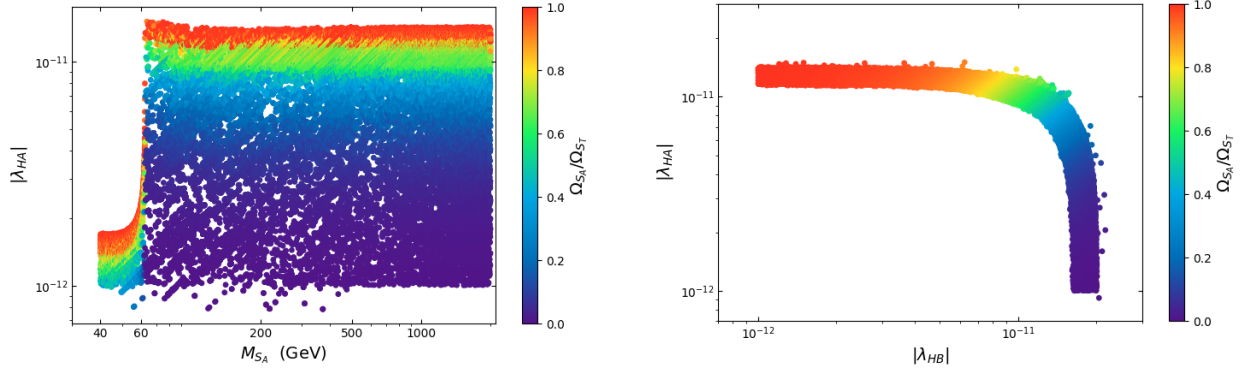


FIG. 2: Parameter space for the FIMP–FIMP regime. **Left:** Standard freeze-in scaling for S_A in the limit where it dominates the total relic abundance, and its progressive deformation as S_B becomes non-negligible. **Right:** Correlation between the portal couplings λ_{HA} and λ_{HB} , colour-coded by the fractional abundance. Points near the diagonal correspond to comparable contributions from both components and populate a characteristic curved band in the $(\lambda_{HA}, \lambda_{HB})$ plane.

2. S_B (WIMP) diluted by S_A (FIMP)

In this mixed stable scenario, the real scalar S_B is the thermal component, interacting with the Standard Model through the Higgs portal coupling λ_{HB} , while the complex scalar S_A remains feebly coupled and is produced non-thermally via freeze-in. Although S_A never thermalises with the SM bath, the final relic-density composition can still be reshaped by intra-dark reactions, so that the direct-detection signal of the WIMP component is effectively rescaled by its fractional abundance.

The viable parameter space is shown in Fig. 3. The left panel displays the rescaled spin-independent cross section, $\xi_{S_B} \sigma_{S_B}^{\text{SI}}$, as a function of the WIMP mass. As in single-component Higgs-portal models, viable points are largely concentrated around the Higgs-resonance region, $M_{S_B} \simeq M_h/2$ (see, e.g., Ref. [38]). In our mixed setup this trend is further accentuated because we restrict the dark-sector couplings to preserve the non-thermal nature of the S_A population, which limits the efficiency of additional depletion channels for the thermal component away from resonance. As a result, annihilation through the Higgs pole becomes the most effective way to obtain an acceptable relic fraction for S_B while remaining below the LZ bound.

A key qualitative difference with respect to single-component realisations arises from the multi-component nature of the dark sector. As shown in the right panel of Fig. 3, the WIMP S_B contributes only a fraction of the total relic density, $\xi_{S_B} \equiv \Omega_{S_B}/\Omega_{\text{tot}}$, with the remainder carried by the feebly interacting component. Parameter points that would be excluded if S_B were required to saturate

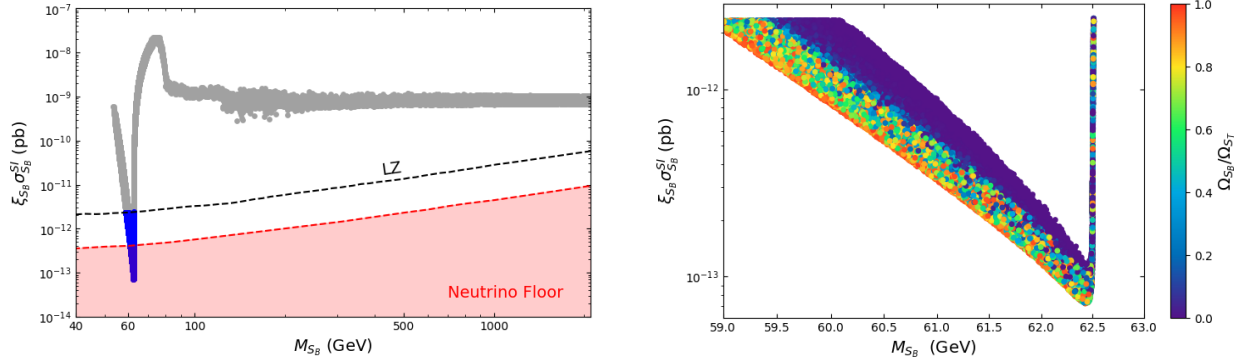
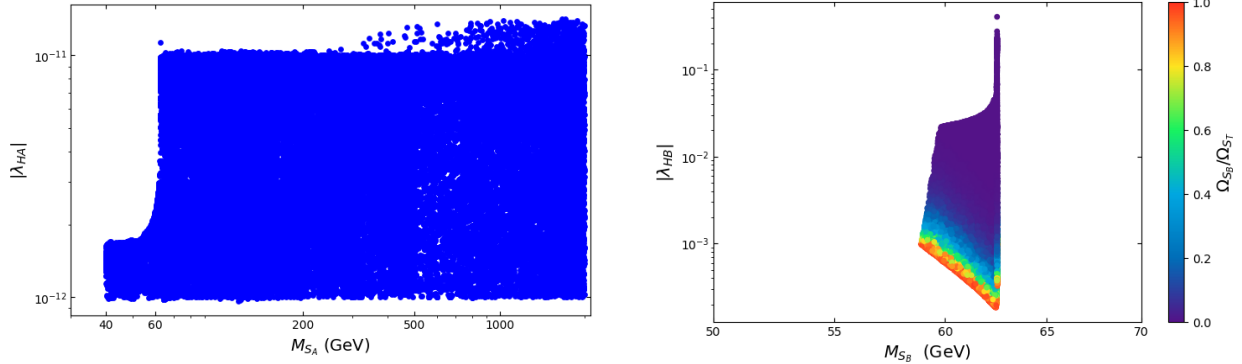


FIG. 3: Direct-detection prospects for the mixed stable scenario with S_B as a WIMP and S_A as a FIMP. All points satisfy the Planck constraint on the total relic abundance, $\Omega_{\text{tot}} h^2$. **Left:** Rescaled spin-independent cross section $\xi_{S_B} \sigma_{S_B}^{\text{SI}}$ as a function of the WIMP mass. Gray points are excluded by the current LZ limit (dashed black line), while blue points remain viable. Viable points cluster around the Higgs-resonance region $M_{S_B} \simeq M_h/2$. **Right:** Fractional contribution of the WIMP component, $\Omega_{S_B}/\Omega_{\text{tot}}$, highlighting the dilution of the direct-detection rate by the FIMP component.

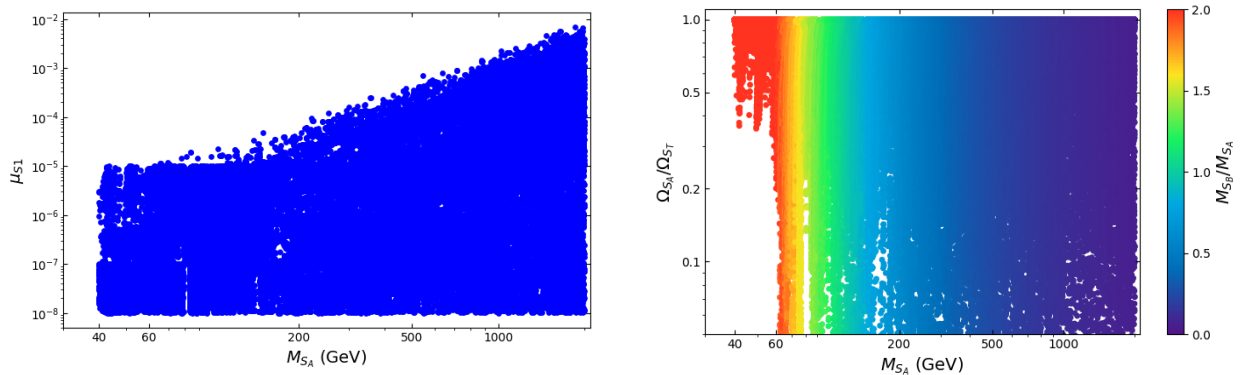
the full dark matter density are therefore recovered once the relic density is shared between the two species.

The structure of the portal couplings is shown in Fig. 4a. The FIMP coupling λ_{HA} follows the characteristic freeze-in scaling familiar from single-component analyses Ref. [37], while the WIMP coupling λ_{HB} exhibits the standard Higgs-portal pattern Ref. [38], with viable points concentrated near the Higgs resonance. Relative to the single-component case, however, both couplings can access wider regions of parameter space because the relic-density requirement and the direct-detection bound are partially decoupled by the multi-component rescaling. In contrast to the two-WIMP \mathbb{Z}_{2n} scenarios studied in Refs. [23, 24], the present mixed thermal/non-thermal setup naturally allows both fields to contribute sizeable fractions of the total abundance.

The interplay between the two sectors is further illustrated in Fig. 4b. The left panel shows a positive correlation between the FIMP mass M_{S_A} and the semi-annihilation coupling μ_{S1} , consistent with the expectation that heavier feebly coupled states typically require stronger intra-dark interactions to achieve the observed total abundance in coupled systems (see, e.g., Refs. [23, 24] for related behaviour in two-WIMP setups). The right panel demonstrates that the FIMP component can dominate the total relic density across a broad mass range, which efficiently suppresses the direct-detection signal since most of the dark matter resides in a component that is effectively invisible to current experiments.



(a) Viable parameter space projected onto the Higgs-portal couplings for the mixed stable scenario (S_A FIMP, S_B WIMP), with all points satisfying the Planck constraint on the total relic abundance. **Left:** λ_{HA} versus M_{S_A} . The freeze-in scaling is preserved, but the allowed band widens since S_A is not required to account for the full density. **Right:** λ_{HB} versus M_{S_B} . Viable points concentrate near $M_{S_B} \simeq M_h/2$, while the rescaling by ξ_{S_B} relaxes the direct-detection exclusion relative to the single-component case.



(b) Correlations involving the dark-sector interaction and the relic-density composition in the mixed stable scenario. **Left:** M_{S_A} versus μ_{S1} . Larger M_{S_A} tends to correlate with larger μ_{S1} , reflecting the increasing relevance of intra-dark processes in the coupled evolution. **Right:** $\Omega_{S_A}/\Omega_{\text{tot}}$ versus M_{S_A} , colour-coded by M_{S_B}/M_{S_A} , showing that the FIMP component can dominate over a broad mass range.

FIG. 4: Parameter-space correlations for the stable mixed scenario with S_A as a FIMP and S_B as a WIMP.

In summary, the mixed FIMP–WIMP configuration opens up regions of parameter space that are excluded in single-component Higgs-portal models. This occurs because the relic-density requirement and the direct-detection bound become partially decoupled once the total abundance is shared between a thermal WIMP and a feebly interacting FIMP, yielding a phenomenologically viable two-component realisation in which both fields play an active role in setting the cosmological abundance.

3. S_A (WIMP) diluted by S_B (FIMP)

We now consider the mixed stable configuration with interchanged roles relative to the previous subsection: the complex scalar S_A is the thermal WIMP, coupled to the SM through the Higgs portal λ_{HA} , while the real scalar S_B remains feebly interacting and is produced via freeze-in through λ_{HB} . The viable points displayed in Fig. 5 exhibit the same underlying mechanism as before: the direct-detection rate of the WIMP component is effectively suppressed by its relic-density fraction $\xi_{S_A} \equiv \Omega_{S_A}/\Omega_{\text{tot}}$ once the total abundance is shared with a FIMP.

The parameter space is nevertheless more kinematically compressed. Stability requires $M_{S_B} < 2M_{S_A}$, so once the interplay of the relic-density requirement with the LZ bound concentrates viable points near the Higgs pole, $M_{S_A} \simeq M_h/2$, the FIMP mass is restricted to $M_{S_B} \lesssim M_h$. As a consequence, both dark states are confined to electroweak-scale masses, in contrast to the S_B -WIMP/ S_A -FIMP realisation where the feebly coupled state could extend to substantially larger masses. This compression also makes the scenario particularly predictive: viable points accumulate in a narrow band around the Higgs pole and $M_{S_B} \lesssim M_h$.

Despite the reduced mass range, the qualitative phenomenology remains the same. The total relic abundance is shared between two stable components, so the WIMP is not required to saturate Ω_{DM} on its own. This again reopens regions that would be excluded in a single-component Higgs-portal setup, while maintaining a genuinely two-component relic-density composition.

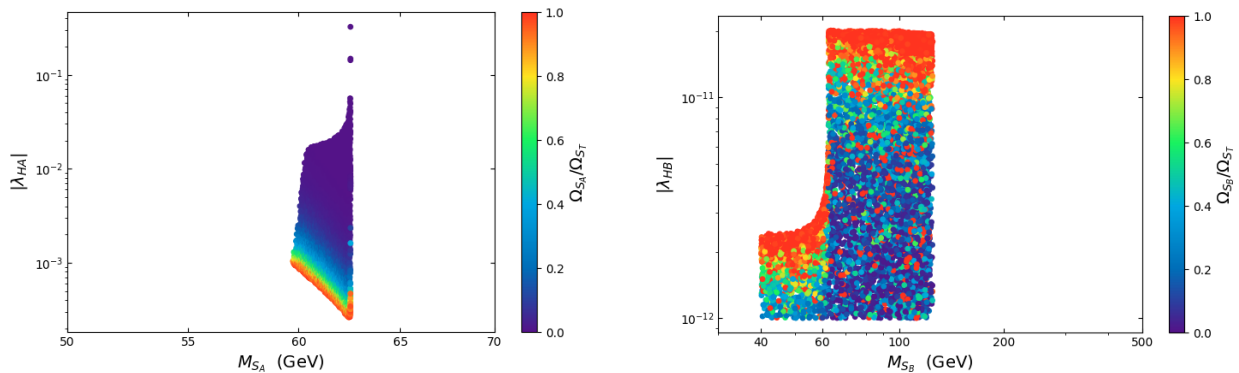


FIG. 5: Viable parameter space for the mixed stable scenario with S_A as a WIMP and S_B as a FIMP. **Left:** (M_{S_A}, λ_{HA}) plane, colour-coded by the WIMP fractional abundance $\Omega_{S_A}/\Omega_{\text{tot}}$. **Right:** (M_{S_B}, λ_{HB}) plane, colour-coded by the FIMP fractional abundance $\Omega_{S_B}/\Omega_{\text{tot}}$. Relative to Fig. 4a, stability ($M_{S_B} < 2M_{S_A}$) combined with the Higgs-pole clustering of viable points ($M_{S_A} \simeq M_h/2$) confines S_B to $M_{S_B} \lesssim M_h$.

In summary, the mixed stable scenario with a WIMP-like S_A is more tightly constrained than its counterpart because stability enforces an upper bound on the FIMP mass once S_A sits near the Higgs resonance. It nevertheless preserves the same key feature: a shared relic abundance that dilutes the WIMP signal and weakens direct-detection exclusions relative to single-component Higgs-portal models.

B. Unstable Scenarios

We now turn to the unstable regime, characterised by the mass hierarchy $M_{S_B} > 2M_{S_A}$, for which the heavier state S_B is no longer cosmologically stable. The decay channel $S_B \rightarrow S_A S_A$ becomes kinematically open. This qualitatively changes the coupled Boltzmann evolution: the final dark matter abundance (ultimately $\Omega_{\text{tot}} \rightarrow \Omega_{S_A}$) is not determined solely by annihilations and scatterings with the SM bath, but can receive an additional non-thermal contribution from the decay of the heavier state.

A key point in these decay-mediated regimes is that the parent abundance can be phenomenologically relevant even if the parent does *not* survive until today. In practice, S_B may contribute negligibly to the present-day energy density, yet still *reshape* the final Ω_{S_A} by transferring its comoving number density into the stable species at late times. In other words, what matters is not the relic abundance of S_B *today*, but the amount of S_B present when the decay occurs and the resulting transfer into S_A after (or alongside) the standard production of S_A . This injection-driven modification of the final relic density is less commonly emphasised in the multi-component Higgs-portal literature and is one of the distinctive aspects of the present \mathbb{Z}_4 setup.

Two limiting non-thermal mechanisms arise depending on the thermal history of the parent state S_B . If S_B thermalises with the SM plasma and freezes out before decaying, the scenario realises the classic *SuperWIMP* mechanism: a WIMP-like parent sets an intermediate abundance through freeze-out and subsequently transfers it to the stable daughter via late decays. If instead S_B remains feebly coupled and is produced via freeze-in, two non-thermal realisations emerge depending on the thermal nature of the daughter state S_A . When S_A thermalises, the late decays $S_B \rightarrow S_A S_A$ provide a source term on top of the WIMP dynamics (*injection-assisted freeze-out*, i.e. “injection freeze-in”). Conversely, if S_A is also feebly coupled, the relic density is set by a purely non-thermal production-and-decay chain (*sequential freeze-in with an unstable parent*, corresponding to a “SuperFIMP”-like limit²), where the decay step can still contribute non-negligibly to the final

² The label “SuperFIMP” is sometimes used informally in the literature/seminar jargon for scenarios in which a

Ω_{S_A} . We analyse these possibilities in turn.

1. The SuperWIMP mechanism (WIMP parent)

In the SuperWIMP regime Refs. [40, 41] (see also Refs. [15, 34] for related mixed WIMP/FIMP model implementations), the parent state S_B has sizeable interactions with the SM bath ($\lambda_{HB} \gtrsim 10^{-4}$), thermalises in the early Universe, and undergoes a conventional freeze-out. Unlike a stable WIMP, however, S_B is unstable and subsequently decays into the feebly interacting daughter S_A through $S_B \rightarrow S_A S_A$, so that the present-day dark matter is entirely carried by S_A .

The final abundance of S_A then receives two conceptually distinct contributions. First, there is the direct freeze-in component sourced by the thermal bath through the feeble portal λ_{HA} . Second, there is an *inherited* contribution from the late decay of the frozen-out S_B population, which transfers comoving number density into S_A at temperatures well below the freeze-out scale. This contribution can be numerically important even though S_B itself becomes cosmologically irrelevant at late times.

The corresponding evolution of comoving number densities is illustrated in the left panel of Fig. 6. After freeze-out, the parent abundance Y_{S_B} (black curves) is approximately constant until decays become efficient; at that point it decreases, while Y_{S_A} (blue curves) increases due to the non-thermal injection. Solid and dashed curves refer to the benchmark choices given in the caption. Under the standard assumption that each decay produces two S_A quanta, $\text{BR}(S_B \rightarrow S_A S_A) \simeq 1$, and that post-injection depletion of S_A is negligible, the resulting relic density can be estimated as

$$\Omega_{S_A} \simeq \Omega_{S_A}^{\text{freeze-in}} + \frac{2M_{S_A}}{M_{S_B}} \Omega_{S_B}^{\text{freeze-out}}. \quad (19)$$

The first term captures the direct freeze-in yield, while the second encodes the late transfer of the frozen-out parent abundance into the stable daughter. This two-source origin of Ω_{S_A} is the defining hallmark of the SuperWIMP mechanism.

A central phenomenological implication is the partial decoupling between relic-density production and direct-detection probes. The final Ω_{S_A} is controlled mainly by the freeze-out dynamics of S_B (set primarily by λ_{HB} , together with the decay rate), whereas direct detection is sensitive only to the Higgs-portal coupling of the *stable* particle, λ_{HA} . Since S_A remains feebly coupled in this regime, the predicted spin-independent rate is far below current sensitivities (e.g. LZ), independently of the value of λ_{HB} .

feebly produced (freeze-in) parent decays at late times and can contribute to the final DM abundance, in particular when the daughter state is also feebly coupled. See, e.g., Ref. [39] for an explicit use of the term.

This decoupling is manifest in the right panel of Fig. 6. In single-component freeze-in, reproducing Ω_{DM} enforces a tight correlation between M_{S_A} and λ_{HA} Ref. [37]. Here, however, viable points populate regions with extremely small portal couplings ($\lambda_{HA} \ll 10^{-11}$) that would otherwise lead to severe underproduction: the missing abundance is compensated by the decay-fed contribution from the WIMP parent. This deformation of the usual freeze-in correlation is therefore *not* driven by feeble dynamics alone, but by the late-time conversion of a thermally produced freeze-out population into the stable FIMP-like state. This distinction will be useful when contrasting the present case with the purely feeble sequential-production scenario discussed next.

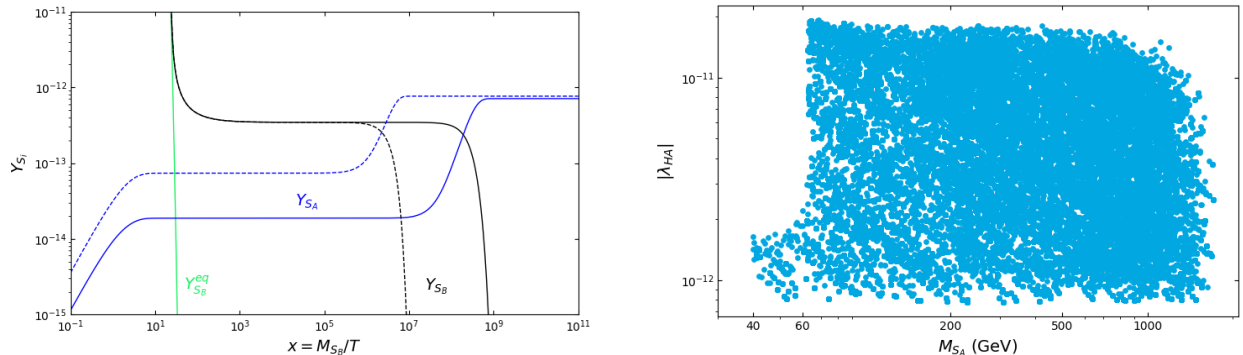


FIG. 6: **Left:** Evolution of comoving number densities in the SuperWIMP scenario. The frozen-out abundance of the parent S_B (black) decreases at late times due to decay, while the daughter abundance of S_A (blue) receives a corresponding non-thermal injection. The parameters are fixed to $M_{S_A} = 6.42 \times 10^2$ GeV, $M_{S_B} = 1.50 \times 10^3$ GeV, $\lambda_{AB} = 2.24 \times 10^{-12}$ and $\lambda_{HB} = 0.416$, with two representative choices for the feeble couplings: $\mu_{S_1} = 1.31 \times 10^{-12}$ GeV and $\lambda_{HA} = 2.49 \times 10^{-12}$ (solid), and $\mu_{S_1} = 1.31 \times 10^{-10}$ GeV and $\lambda_{HA} = 5.49 \times 10^{-12}$ (dashed). **Right:** Viable parameter space for the stable daughter S_A . The standard single-component freeze-in correlation is strongly relaxed, with viable points extending well below the usual freeze-in band due to the additional contribution from the decay of the WIMP parent.

2. Injection and sequential freeze-in with late dark-sector decays

When the parent particle S_B is feebly coupled to the SM bath, the final dark matter abundance is set by freeze-in production followed by a decay within the dark sector, $S_B \rightarrow S_A S_A$. We consider two qualitatively distinct realisations depending on whether the stable daughter S_A thermalises with the visible plasma. While the resulting projections on (M_{S_A}, λ_{HA}) may resemble the SuperWIMP case,

the underlying dynamics is different: here the relic density is shaped by a *sequential* non-thermal history, with no thermally produced WIMP parent driving the late injection.

a. Injection freeze-in: S_B (FIMP) \rightarrow S_A (WIMP). In this configuration the unstable state S_B is produced via freeze-in and decays into a stable WIMP-like daughter S_A . The latter can thermalise and undergo standard freeze-out, but its final abundance receives an additional contribution from the late decay of S_B , which injects S_A quanta at temperatures well below the freeze-out epoch (left panel of Fig. 7). Consequently, the relic density of S_A is not controlled solely by its annihilation efficiency, but also by the yield and lifetime of the decaying FIMP parent.

This late-time injection alters the usual mapping between the portal coupling λ_{HA} and the relic abundance. In particular, regions that would be *under-abundant* in standard single-component freeze-out can become viable because the injected population compensates for efficient early depletion. In the (M_{S_A}, λ_{HA}) plane, this effect deforms the familiar Higgs-resonance funnel, opening viable solutions that are absent in the conventional freeze-out picture (right panel of Fig. 7).

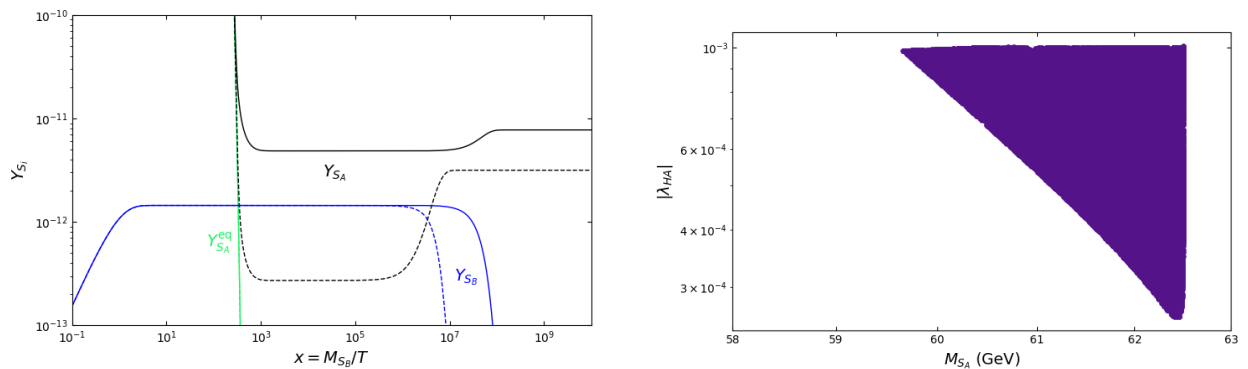


FIG. 7: Injection freeze-in scenario in which an unstable FIMP parent S_B decays into a stable WIMP daughter S_A . **Left:** Evolution of comoving number densities. The WIMP-like abundance of S_A (black) initially follows standard freeze-out, but receives a late non-thermal injection from the decay of the FIMP parent S_B (blue). The parameters are fixed to $M_{S_A} = 6.04 \times 10^1$ GeV, $M_{S_B} = 7.54 \times 10^2$ GeV, $\lambda_{AB} = 2.08 \times 10^{-12}$ and $\lambda_{HB} = -1.46 \times 10^{-12}$, with two representative choices: $\mu_{S_1} = 2.08 \times 10^{-12}$ GeV and $\lambda_{HA} = 9.49 \times 10^{-4}$ (solid), and $\mu_{S_1} = 2.08 \times 10^{-11}$ GeV and $\lambda_{HA} = 4.55 \times 10^{-3}$ (dashed). **Right:** Viable WIMP parameter space in the (M_{S_A}, λ_{HA}) plane. Late injection from S_B deforms the standard Higgs-resonance funnel, allowing viable points that would be under-abundant in conventional single-component freeze-out scenarios.

b. Sequential freeze-in: S_B (FIMP) \rightarrow S_A (FIMP). In this realisation both particles remain out of equilibrium with the SM bath. The parent S_B is first produced via freeze-in and subsequently

decays into $S_A S_A$, so that the final abundance of the stable FIMP S_A is generated through a two-step production chain (Fig. 8).

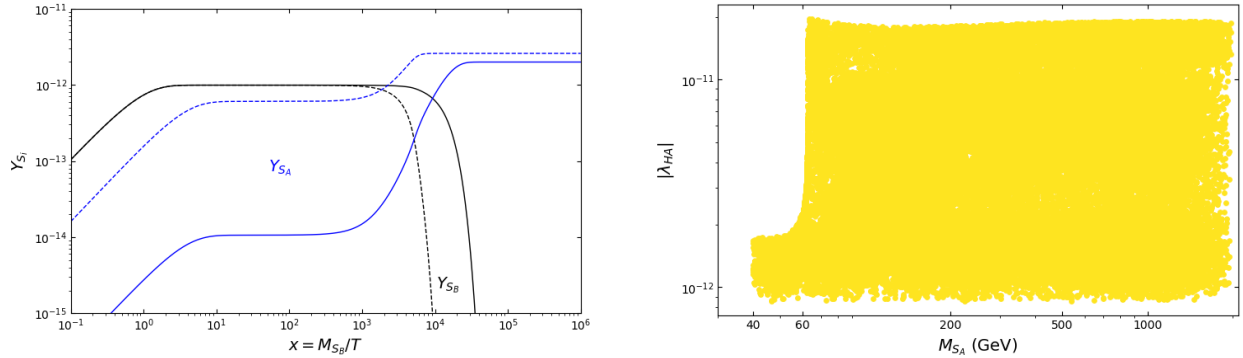


FIG. 8: Sequential freeze-in scenario in which a feebly produced parent S_B decays into the stable FIMP S_A . **Left:** Two-step production of S_A . The parent S_B is produced via freeze-in and later decays into $S_A S_A$, yielding a delayed non-thermal contribution to the final abundance. The parameters are fixed to $M_{S_A} = 2.21 \times 10^2$ GeV, $M_{S_B} = 8.12 \times 10^2$ GeV, $\lambda_{AB} = -8.41 \times 10^{-11}$ and $\lambda_{HB} = 3.33 \times 10^{-11}$, with two representative choices: $\mu_{S_1} = 1.27 \times 10^{-8}$ GeV and $\lambda_{HA} = 1.22 \times 10^{-12}$ (solid), and $\mu_{S_1} = 5.27 \times 10^{-8}$ GeV and $\lambda_{HA} = 9.22 \times 10^{-12}$ (dashed). **Right:** Viable parameter space for the stable FIMP S_A . Compared to standard single-component freeze-in, the usual mass–coupling correlation is relaxed because the relic density depends on both λ_{HA} and the parent yield and lifetime.

As in the SuperWIMP mechanism, sequential production relaxes the direct correlation between the FIMP mass and its portal coupling. However, in the present case the effect arises *without* any thermalised dark-sector state: the relic density of S_A depends not only on λ_{HA} , but also on the freeze-in abundance of S_B and on the decay time controlling the delayed injection. This highlights that similar-looking deformations in (M_{S_A}, λ_{HA}) can originate from dynamically distinct non-thermal histories, and provides a natural route to viable FIMP parameter space beyond the standard single-step freeze-in expectation.

Dedicated discussions of this kind of sequential freeze-in with late decays confined to the dark sector remain relatively scarce, especially for minimal \mathbb{Z}_4 scalar implementations; our results therefore provide a useful benchmark map for this class of non-thermal histories.

V. CONCLUSIONS

We have investigated a renormalisable \mathbb{Z}_4 Higgs-portal dark sector with a complex scalar S_A and a real scalar S_B , emphasising cosmological histories in which one (or both) components depart from thermal equilibrium. The starting motivation was the apparent structural tension found in thermal two-component Higgs portals: even after the standard relic-fraction rescaling, current spin-independent limits (notably LZ) can jointly disfavor large regions that would seem acceptable for each species considered separately. We asked whether this tension should be interpreted as a generic obstacle for \mathbb{Z}_{2n} -stabilised multi-component portals, or mainly as a consequence of enforcing *two thermal* relic histories.

Our results support the second interpretation. Once mixed and non-thermal cosmologies are treated consistently, the \mathbb{Z}_4 Higgs-portal benchmark remains broadly viable. Moving beyond the two-thermal-WIMP assumption substantially enlarges the allowed parameter space and admits regimes in which *both* dark-sector states can contribute appreciably to the present-day DM budget, in contrast to the more restrictive two-WIMP interpretation of the same model. Allowing a feebly coupled component decouples the relic-density requirement from direct detection: the total abundance can be shared with an effectively invisible species and/or receive a contribution from dark-sector decays. The genuinely \mathbb{Z}_4 interactions—conversion, semi-annihilation, and decay/inverse-decay—then control how the final abundance is partitioned and transferred, yielding a phenomenology substantially richer than in single-component Higgs portals, while remaining predictive in a minimal and controlled setup.

We organised the parameter space into six scenarios spanning the stable two-component regime ($M_{S_B} < 2M_{S_A}$) and the decay-mediated regime ($M_{S_B} > 2M_{S_A}$). The key outcomes can be summarised as follows:

- **Stable FIMP–FIMP (Scenario 1).** With feeble portals, neither species thermalises and both abundances arise from freeze-in. Viable points readily realise shared relic partitions, with a characteristic correlation between the portal couplings when $\Omega_{S_A} \simeq \Omega_{S_B}$. Direct searches are essentially insensitive in this limit.
- **Stable mixed WIMP–FIMP (Scenarios 2–3).** Direct-detection limits apply only to the thermal component (with the usual ξ rescaling), while the FIMP-like component is effectively invisible. Sharing the relic density can therefore substantially dilute the WIMP direct-detection signal at fixed Ω_{DM} , with viable solutions typically clustering near the Higgs

resonance for the WIMP-like species. When S_A is the WIMP (Scenario 3), the stability condition $M_{S_B} < 2M_{S_A}$ compresses the allowed FIMP mass range; when S_B is the WIMP (Scenario 2), the FIMP component can extend to higher masses and often dominates the abundance, enhancing the dilution effect.

- **Decay-mediated injection (Scenarios 4–6).** For $M_{S_B} > 2M_{S_A}$ the late-time relic is S_A , but its final abundance can receive an essential contribution from $S_B \rightarrow S_A S_A$ decays. We find three distinct regimes: *SuperWIMP* (Scenario 4), where a thermally produced parent freezes out and later decays into a feebly coupled daughter; *injection freeze-in* (Scenario 5; i.e. injection-assisted freeze-out), where a feebly produced parent injects a WIMP-like daughter and deforms the usual freeze-out funnel; and *sequential freeze-in* (Scenario 6), where both states remain out of equilibrium and the relic is generated through a two-step non-thermal chain. In all cases, late injection relaxes the usual mass–portal correlations and yields viable points that would otherwise underproduce (or be over-depleted in) conventional single-step pictures.

Concerning cosmological consistency, the decay $S_B \rightarrow S_A S_A$ is fully internal to the dark sector. In the viable regions of our scan, the fraction of dark matter sourced by late decays is small enough that structure-formation constraints from free streaming are naturally avoided. This makes the \mathbb{Z}_4 benchmark a concrete target space in which direct detection predominantly probes the thermal component (when present), while the non-thermal regimes motivate complementary searches and cosmological tests sensitive to dark-sector injection and conversion.

ACKNOWLEDGMENTS

We thank A. Pukhov for useful discussions and for assistance with `micrOMEGAs`. B. L. Sánchez-Vega and J. P. Carvalho-Corrêa acknowledge financial support from the National Council for Scientific and Technological Development (CNPq) through Grants No. 311699/2020-0 and No. 141118/2022-9, respectively. B. A. Couto e Silva acknowledges financial support from the Fundação de Amparo à Pesquisa do Estado de Minas Gerais (FAPEMIG) and from the Coordenação de Aperfeiçoamento de Pessoal de Nível Superior (CAPES).

Appendix A: Theoretical Constraints

In this appendix we summarise the bounded-from-below (BFB) conditions and the tree-level perturbative unitarity/perturbativity requirements imposed throughout our numerical analysis. For full derivations of the relevant scalar-scattering matrices and the BFB criteria in the \mathbb{Z}_4 framework, we refer the reader to Ref. [24] and references therein.

1. Perturbative unitarity

Tree-level perturbative unitarity is enforced by requiring that the zeroth partial-wave amplitude for all $2 \rightarrow 2$ scalar scattering processes satisfies $|\Re(a_0)| \leq 1/2$. Following the conventions of Ref. [24], we implement this condition through the conservative bound

$$|\mathcal{M}_i| \leq 8\pi, \quad (\text{A1})$$

for every eigenvalue \mathcal{M}_i of the high-energy scalar-scattering matrices.

Applied to the potential in Eq. (3), this yields the constraints

$$|\lambda_H|, |\lambda_{AB}|, |\lambda_A \pm 3\lambda_{S4}| \leq 4\pi, \quad |\lambda_{HA}|, |\lambda_{HB}| \leq 8\pi. \quad (\text{A2})$$

In addition, the $(hh, S_A S_A^\dagger, S_B S_B)$ sector leads to three eigenvalues $x_{1,2,3}$, given by the real roots of

$$x^3 + A x^2 + B x + C = 0, \quad (\text{A3})$$

with coefficients

$$A = 12\lambda_H + 8\lambda_A + 24\lambda_B, \quad (\text{A4})$$

$$B = 96\lambda_H\lambda_A + 288\lambda_H\lambda_B + 192\lambda_A\lambda_B - 8\lambda_{AB}^2 - 8\lambda_{HA}^2 - 4\lambda_{HB}^2, \quad (\text{A5})$$

$$C = 2304\lambda_H\lambda_A\lambda_B - 96\lambda_H\lambda_{AB}^2 - 32\lambda_A\lambda_{HB}^2 - 192\lambda_B\lambda_{HA}^2 + 32\lambda_{AB}\lambda_{HA}\lambda_{HB}. \quad (\text{A6})$$

We enforce

$$|x_k| \leq 16\pi, \quad k = 1, 2, 3, \quad (\text{A7})$$

again following the normalisation and identical-particle conventions adopted in Ref. [24].

2. Global bounded-from-below condition

Besides the field-axis and pairwise BFB requirements in Eqs. (5)–(8), the potential must remain bounded from below when all three field directions H , S_A , and S_B are simultaneously activated. Using the effective couplings $\bar{\lambda}_{ij}$ defined in Eqs. (6)–(8), the corresponding copositivity condition can be written as

$$2\lambda_{AB}\sqrt{\lambda_H} + 2\lambda_{HA}\sqrt{\lambda_B} + \lambda_{HB}\sqrt{\lambda_A - |\lambda_{S4}|} + 4\sqrt{\lambda_H(\lambda_A - |\lambda_{S4}|)\lambda_B} + \sqrt{2\bar{\lambda}_{HA}\bar{\lambda}_{HB}\bar{\lambda}_{AB}} > 0. \quad (\text{A8})$$

This condition ensures that the quartic part of the potential is non-negative at large field values for arbitrary field directions.

3. Perturbativity

Finally, to ensure the validity of the perturbative expansion, we impose the hard cut

$$|\lambda_i| \leq 4\pi, \quad \lambda_i \in \{\lambda_H, \lambda_A, \lambda_B, \lambda_{HA}, \lambda_{HB}, \lambda_{AB}, \lambda_{S4}\}. \quad (\text{A9})$$

Points failing any of the conditions listed in this appendix are discarded from the analysis.

-
- [1] Planck Collaboration, Aghanim, N., *et al.*, “Planck 2018 results. VI. Cosmological parameters,” *Astron. Astrophys.* **641** (2020) A6, [arXiv:1807.06209](https://arxiv.org/abs/1807.06209) [[astro-ph.CO](https://arxiv.org/archive/astro-ph)].
 - [2] V. C. Rubin and J. Ford, W. Kent, “Rotation of the Andromeda Nebula from a Spectroscopic Survey of Emission Regions,” *Astrophys. J.* **159** (1970) 379–403.
 - [3] Y. Sofue and V. Rubin, “Rotation Curves of Spiral Galaxies,” *Annu. Rev. Astron. Astrophys.* **39** (2001) 137–174, [arXiv:astro-ph/0010594](https://arxiv.org/abs/astro-ph/0010594).
 - [4] D. Clowe, M. Bradac, A. H. Gonzalez, M. Markevitch, S. W. Randall, C. Jones, and D. Zaritsky, “A Direct Empirical Proof of the Existence of Dark Matter,” *Astrophys. J. Lett.* **648** (2006) L109–L113, [arXiv:astro-ph/0608407](https://arxiv.org/abs/astro-ph/0608407).
 - [5] Particle Data Group, “Review of Particle Physics: Dark Matter.” 2023. <https://pdg.lbl.gov/2023/reviews/rpp2022-rev-dark-matter.pdf>. PDG review “Dark Matter”.
 - [6] G. Bertone, D. Hooper, and J. Silk, “Particle dark matter: evidence, candidates and constraints,” *Phys. Rept.* **405** (2005) 279–390, [arXiv:hep-ph/0404175](https://arxiv.org/abs/hep-ph/0404175).
 - [7] G. Jungman, M. Kamionkowski, and K. Griest, “Supersymmetric dark matter,” *Phys. Rept.* **267** (1996) 195–373, [arXiv:hep-ph/9506380](https://arxiv.org/abs/hep-ph/9506380).

- [8] G. Arcadi, A. Djouadi, and M. Raidal, “Dark Matter through the Higgs portal,” *Phys. Rept.* **842** (2020) 1–180, [arXiv:1903.03616 \[hep-ph\]](#).
- [9] B. L. Sánchez-Vega, J. C. Montero, and E. R. Schmitz, “Complex scalar dark matter in a $B - L$ model,” *Phys. Rev. D* **90** no. 5, (2014) 055022, [arXiv:1404.5973 \[hep-ph\]](#).
- [10] B. L. Sánchez-Vega and E. R. Schmitz, “Fermionic dark matter and neutrino masses in a $\mathcal{B} - \mathcal{L}$ model,” *Phys. Rev. D* **92** (2015) 053007, [arXiv:1505.03595 \[hep-ph\]](#).
- [11] A. G. Dias, V. Padovani, K. Kannike, N. Koivunen, J. Leite, and B. L. Sánchez-Vega, “Dark matter in the scale-invariant 3-3-1-1 model,” *Phys. Rev. D* **112** no. 11, (2025) 115017, [arXiv:2501.17914 \[hep-ph\]](#).
- [12] K. M. Zurek, “Multicomponent dark matter,” *Phys. Rev. D* **79** (2009) 115002, [arXiv:0811.4429 \[hep-ph\]](#).
- [13] M. Aoki, M. Duerr, J. Kubo, and H. Takano, “Multicomponent dark matter systems and their observation prospects,” *Phys. Rev. D* **86** (2012) 076015, [arXiv:1207.3318 \[hep-ph\]](#).
- [14] R. Capucha, K. Elyauti, M. Mühlleitner, J. Plotnikov, and R. Santos, “Freeze-in as a complementary process to freeze-out,” *JHEP* **2024** no. 9, (2024) 113, [arXiv:2407.04809 \[hep-ph\]](#).
- [15] G. Bélanger, A. Mjallal, and A. Pukhov, “WIMP and FIMP dark matter in the inert doublet plus singlet model,” *Phys. Rev. D* **106** (2022) 095019, [arXiv:2205.04101 \[hep-ph\]](#).
- [16] S. Profumo, K. Sigurdson, and L. Ubaldi, “Can we discover dual-component thermal WIMP dark matter?,” *JCAP* **12** (2009) 016, [arXiv:0907.4374 \[hep-ph\]](#).
- [17] S. Esch, M. Klasen, and C. E. Yaguna, “A minimal model for two-component dark matter,” *JHEP* **09** (2014) 108, [arXiv:1406.0617 \[hep-ph\]](#).
- [18] K. R. Dienes, J. Kumar, and B. Thomas, “Direct detection of dynamical dark matter,” *Phys. Rev. D* **86** (2012) 055016, [arXiv:1208.0336 \[hep-ph\]](#).
- [19] K. Griest and D. Seckel, “Three exceptions in the calculation of relic abundances,” *Phys. Rev. D* **43** (1991) 3191–3203.
- [20] F. D’Eramo and J. Thaler, “Semi-annihilation of dark matter,” *JHEP* **06** (2010) 109, [arXiv:1003.5912 \[hep-ph\]](#).
- [21] G. Bélanger, K. Kannike, A. Pukhov, and M. Raidal, “ \mathbb{Z}_3 scalar singlet dark matter,” *JCAP* **01** (2013) 022, [arXiv:1211.1014 \[hep-ph\]](#).
- [22] C. E. Yaguna and Ó. Zapata, “Multi-component scalar dark matter from a \mathbb{Z}_N symmetry: A systematic analysis,” *JHEP* **03** (2020) 109, [arXiv:1911.05515 \[hep-ph\]](#).
- [23] C. E. Yaguna and Ó. Zapata, “Two-component scalar dark matter in \mathbb{Z}_{2n} scenarios,” *JHEP* **10** (2021) 185, [arXiv:2106.11889 \[hep-ph\]](#).
- [24] J. P. Carvalho-Corrêa, I. M. Pereira, B. L. Sánchez-Vega, and A. C. D. Viglioni, “Theoretical and experimental constraints on \mathbb{Z}_{2n} multi-component dark matter models,” *Eur. Phys. J. C* **85** (2025) 1353.
- [25] LZ Collaboration, “Dark Matter Search Results from 4.2 Tonne-Years of Exposure of the LUX-ZEPLIN (LZ) Experiment,” *Phys. Rev. Lett.* **135** (2025) 011802, [arXiv:2410.17036 \[hep-ex\]](#).

- [26] K. Kannike, “Vacuum stability conditions from copositivity criteria,” *Eur. Phys. J. C* **72** (2012) 2093.
- [27] ATLAS Collaboration, “Combination of searches for invisible decays of the Higgs boson using 139 fb⁻¹ of proton-proton collision data at $\sqrt{s} = 13$ TeV collected with the ATLAS experiment,” *Phys. Lett. B* **842** (2023) 137963.
- [28] R. H. Cyburt, B. D. Fields, K. A. Olive, and T.-H. Yeh, “Big bang nucleosynthesis: Present status,” *Rev. Mod. Phys.* **88** (Feb, 2016) 015004.
- [29] M. Kawasaki, K. Kohri, and T. Moroi, “Big-bang nucleosynthesis and hadronic decay of long-lived massive particles,” *Phys. Rev. D* **71** (2005) 083502, [arXiv:astro-ph/0408426v2](#).
- [30] K. Jedamzik, “Big bang nucleosynthesis constraints on hadronically and electromagnetically decaying relic neutral particles,” *Phys. Rev. D* **74** (2006) 103509, [arXiv:hep-ph/0604251](#).
- [31] J. Decant, J. Heisig, D. Hooper, and L. Lopez-Honorez, “Lyman- α constraints on freeze-in and superWIMPs,” *JCAP* **03** (2022) 041, [arXiv:2111.09321 \[hep-ph\]](#).
- [32] M. Viel, G. D. Becker, J. S. Bolton, and M. G. Haehnelt, “Warm dark matter as a solution to the small scale crisis: New constraints from high redshift Lyman- α forest data,” *Phys. Rev. D* **88** (2013) 043502, [arXiv:1306.2314 \[astro-ph.CO\]](#).
- [33] V. Iršič, M. Viel, *et al.*, “New constraints on the free-streaming of warm dark matter from intermediate and small scale Lyman- α forest data,” *Phys. Rev. D* **96** (2017) 023522, [arXiv:1702.01764](#).
- [34] C. E. Yaguna and Ó. Zapata, “Minimal model of fermion FIMP dark matter,” *Phys. Rev. D* **109** (2024) 015002.
- [35] G. Alguero, G. Belanger, F. Boudjema, S. Chakraborti, A. Goudelis, S. Kraml, A. Mjallal, and A. Pukhov, “micrOMEGAs 6.0: N-component dark matter,” *Comput. Phys. Commun.* **299** (2024) 109133, [arXiv:2312.14894 \[hep-ph\]](#).
- [36] M. Pandey, D. Majumdar, and K. P. Modak, “Two Component Feebly Interacting Massive Particle (FIMP) dark matter,” *JCAP* **06** (2018) 023.
- [37] C. E. Yaguna, “The singlet scalar as FIMP dark matter,” *JHEP* **08** (2011) 060, [arXiv:1105.1654 \[hep-ph\]](#).
- [38] P. Athron, C. Balázs, T. Bringmann, A. Buckley, M. Chruszcz, J. Conrad, *et al.*, “Status of the scalar singlet dark matter model,” *Eur. Phys. J. C* **77** (2017) 568, [arXiv:1705.07931 \[hep-ph\]](#).
- [39] L. Covi and S. Khan, “Axion and FIMP dark matter in a $U(1)$ extension of the standard model,” *JCAP* **09** (2022) 064, [arXiv:2205.10150 \[hep-ph\]](#).
- [40] J. L. Feng, A. Rajaraman, and F. Takayama, “Superweakly Interacting Massive Particles,” *Phys. Rev. Lett.* **91** (2003) 011302, [arXiv:hep-ph/0302215](#).
- [41] J. L. Feng, A. Rajaraman, and F. Takayama, “Superweakly interacting massive particle dark matter signals from the early universe,” *Phys. Rev. D* **68** (2003) 063504.